New Capillary Number Definition for Micromodels

The Impact of Pore Microstructure

Tang, Jinyu; Smit, Michiel; Vincent-Bonnieu, Sebastien; Rossen, William R.

DOI
10.1029/2018WR023429

Publication date
2019

Document Version
Final published version

Published in
Water Resources Research

Water Resources Research

RESEARCH ARTICLE
10.1029/2018WR023429

Special Section:
Hydrology delivers Earth System Sciences to Society (HESSS4): Improving and Integrating Knowledge across Disciplines on Global Energy, Water and Carbon Cycles

New Capillary Number Definition for Micromodels: The Impact of Pore Microstructure

Jinyu Tang[1], Michiel Smit[1], Sebastien Vincent-Bonnieu[1,2], and William R. Rossen[1]

[1]Department of Geoscience and Engineering, Delft University of Technology, Delft, Netherlands, [2]Shell Global Solutions International, Rijswijk, Netherlands

Abstract A new capillary number (N_{ca}) definition is proposed for 2-D etched micromodels. We derive the new definition from a force balance on a nonwetting ganglion trapped by capillarity. It incorporates the impact of pore microstructure on mobilization. The geometrical factors introduced can be estimated directly from image analysis of the pore network etched in the micromodel, without conducting flow experiments. The improved fit of the new N_{ca} to published data supports its validity. The new definition yields a consistent trend in the capillary-desaturation curve. The conventional N_{ca} definitions proposed for porous rock give a large scatter in the capillary-desaturation curve for data in micromodels. This is due to the different type of flow in micromodels, as 2-D networks, relative to 3-D geological porous media. In particular, permeability is dominated by channel depth in micromodels with shallow depth of etching, and generally, there is no simultaneous multiphase flow under capillary-dominated conditions. Applying the conventional definitions to results in micromodels may lead to misleading conclusions for fluid transport in geological formations.

Plain Language Summary Mobilization or trapping of fluids in porous media, fundamentally, is a result of a force competition. Numerous studies investigate mobilization efficiency using the capillary number (N_{ca}), which represents a ratio of driving force for mobilization, that is, pressure or hydrostatic effects of gravity, to capillary resistance. The conventional N_{ca} definitions were initially proposed for 3-D porous media, yet many experimental studies use these definitions for 2-D networks. Experimental observations and theoretical analysis show that flow in a 2-D pore network, for example, a microfluidic device, is very different from that in 3-D porous rock. We here propose a new definition of N_{ca} to describe the efficiency of one phase displaced by another in a microfluidic device. The new definition is derived from a force balance on a trapped ganglion. The validity of the new definition is experimentally tested using data from micromodels in the literature. The new N_{ca} definition, as an indicator for mobilization, may be applied to microfluidic studies of a variety of processes across the fields of groundwater, energy, and climate: removal of Nonaqueous Phase Liquid contaminants from aquifers and soils; enhanced recovery of oil in reservoirs; or trapping efficiency of CO_2 in Carbon Capture, Utilization, and Storage.

Key Points:
- A new capillary number (N_{ca}) definition, derived from a force balance on a ganglion trapped by capillarity, is proposed for micromodels
- The improved fit of the new N_{ca} to published data supports its validity by yielding a consistent trend in the capillary-desaturation curve
- Applying conventional N_{ca} definitions to micromodel results may lead to incorrect conclusions for fluid transport in geological formations

Correspondence to:
J. Tang,
J.Tang-4@tudelft.nl

Citation:
Tang, J., Smit, M., Vincent-Bonnieu, S., & Rossen, W. R. (2019). New capillary number definition for micromodels: The impact of pore microstructure. *Water Resources Research*, *55*. https://doi.org/10.1029/2018WR023429

Received 6 JUN 2018
Accepted 21 DEC 2018
Accepted article online 2 JAN 2019

1. Introduction

The transport of fluids in porous media, on the macroscopic scale, is captured by permeability and relative-permeability functions. One key focus of fluid transport in porous media, either in practical applications or in lab and theoretical studies, is the mobilization or trapping efficiency of the nonwetting phase. For instance, numerous efforts have been made to enhance the recovery of oil in a reservoir (Lake et al., 2014) or to maximize the removal of Nonaqueous Phase Liquid (NAPL) in contaminated ground water and soil (Geistlinger et al., 2009; Jeong & Corapcioglu, 2005; Johnson et al., 2001; Kao et al., 2008). Other recent studies have attempted to increase the entrapment efficiency of CO_2 in Carbon Capture, Utilization, and Storage (CCUS), to relieve the impact of CO_2 on global climate (Iglauer, Wülling, et al., 2011, Iglauer, Paluszny, et al., 2011; Juanes et al., 2006). The correlation between nonwetting-phase saturation (S_{nw}) and capillary number (N_{ca}), initially realized by Bethel and Calhoun (1953), has long been widely used to analyze the mobilization of nonwetting phase in geological formations. The plot of S_{nw} against N_{ca} is usually referred to as the capillary-desaturation curve (CDC). This type of curve, in combination with other curves, that is, of relative permeability and capillary pressure (Green & Willhite, 1998; Lake et al., 2014), is thought to be among the most fundamental curves in understanding the dynamics of fluid transport in geological formations. The usefulness of the CDC depends on demonstrating a consistent relationship between S_{nw} and N_{ca},

regardless of all the complexities in rock and fluid properties, including pore geometry and ganglion-length distribution. This consistency makes the capillary number an important indicator for the mobilization or trapping efficiency of the nonwetting phase in the processes discussed above.

The conventional N_{ca} definitions were all originally proposed for 3-D porous rock. These definitions have been applied to 2-D pore networks, ignoring the very-different flow between the two types of porous media. Our study aims at proposing a new mobilization condition for nonwetting phase in 2-D pore networks, in particular micromodels. The new criterion is not intended to equate microfluidics to 3-D porous media. If one attempts to extrapolate microfluidic experimental results to interpret behavior in 3-D porous media, the conventional N_{ca} definitions can lead to incorrect conclusions for fluid transport.

Several capillary-number definitions for geological porous rock have been reported in the literature. Generally, most of the definitions fall into two major simplified forms, either in terms of velocity (Foster, 1973; Green & Willhite, 1998) or macroscopic pressure gradient (Brownell & Katz, 1947), as in equations (1) and (2):

$$N_{ca} = \frac{v\mu}{\sigma}, \tag{1}$$

$$N_{ca} = \frac{k|\nabla p|}{\sigma}, \tag{2}$$

where v and μ are the interstitial velocity and viscosity of the displacing fluid, respectively, σinterfacial tension between the displacing and displaced fluids, k permeability, and $|\nabla p|$ the magnitude of macroscopic pressure gradient. All the other definitions are based on the two major forms above. Moore and Slobod (1955), in their analysis using a pore-doublet model, introduced ($\cos\theta$) into the denominator of equation (1) to account for wettability. Abrams (1975) modified the definition in equation (1), using the interstitial velocity of displacing phase and taking the viscosities of both phases into account. Some definitions adjusted the form of equation (2) by including ($\cos\theta$) into the denominator (Dombrowski & Brownell, 1954; Reed & Healy, 1977). Pennell et al. (1996) used the permeability to the displacing phase in equation (2) rather than absolute permeability, which, in addition, introduces the relative permeability. Since the relative permeability varies with S_{nw}, the value of which in turn depends on N_{ca}, the definition in equation (2) involving the relative permeability is impractical for implementation in numerical simulations (Sheng, 2010).

The most commonly used definition of capillary number is in equation (1). That in equation (2) is based on a simplified force balance. Through the relation $v\mu = (kk_{rw}\nabla p)/\varphi$, based on Darcy's Law, the first definition in equation (1) is related to that in equation (2) via

$$(N_{ca})_2 = \frac{(N_{ca})_1}{(k_{rw}/\varphi)}, \tag{3}$$

where subscripts 1 and 2 denote the definitions in equations (1) and (2), respectively, and k_{rw} represents the relative permeability to the wetting (continuous) phase. The definition in equation (2) is, we think, more directly related to the physics of mobilization. It can be derived from a force balance on a trapped nonwetting ganglion, with the crucial assumption that pore length and pore-throat width each scale with the square root of permeability (Sheng, 2010).

Numerous studies have attempted to understand the physics behind the CDC in more detail. For instance, Yeganeh et al. (2016) investigated the relation between S_{nw} and N_{ca} through the ganglion-length distribution and a critical ganglion length that is inversely related to N_{ca} (Larson et al., 1977). A variety of other expressions exists that describe the effect of fluid properties on mobilization (Al-Shalabi et al., 2014; Bethel & Calhoun, 1953; Franklin, 1994; Pope et al., 2000; Rodríguez de Castro et al., 2015).

On a microscopic scale, the transport of fluids in porous media depends on the geometry and topology of the network of pore throats and bodies (Chatzis et al., 1983; Ross & Kovscek, 2002). However, the link between permeability and pore geometry is not the same for all porous media. In particular, permeability in etched micromodels of shallow depth is dominated by the channel depth, rather than the geometrical factors that control trapping, for example, pore-throat width and pore-body diameter, as in porous rock. In addition, it

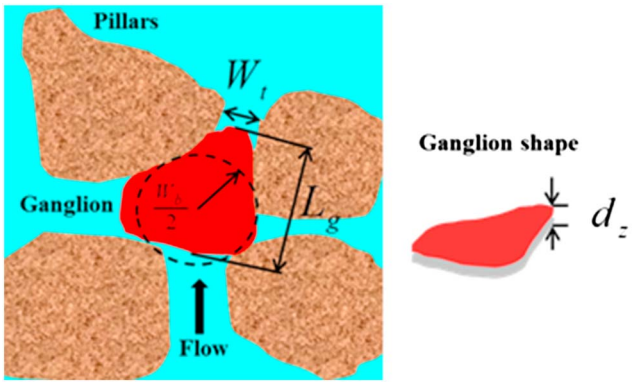

Figure 1. Representation of a nonwetting ganglion trapped by capillarity in a micromodel: (left) top view of a horizontally mounted micromodel; (right) 3-D view of the ganglion shaped by the pore space with relatively shallow etching, where the ganglion is shown as flat due to uniform channel depth.

has long been known (Chatzis & Dullien, 1977; Mohanty et al., 1987; Wilkinson, 1984) that simultaneous multiple phase flow under capillary-dominated conditions is a feature of 3-D pore networks, but not true in general for 2-D networks. Thus, the distribution of residual nonwetting phase is expected to be very different.

Equation (1) indicates an immediate problem in applying a definition of N_{ca} that involves relative permeability to both 3-D pore networks and micromodels. Since 2-D pore networks usually do not allow simultaneous, capillary-dominated multiphase flow, one important implication is that the relative-permeability functions for microfluidic devices are markedly different from those for rock. In the case of water displacing oil in a water-wet micromodel, the onset of trapping of oil marks the beginning of water flowing as a continuous phase, which is a condition where $k_{rw} \sim 0$. This is because the two phases cannot each percolate through an interconnected network in a displacement (Chatzis & Dullien, 1977; Mohanty et al., 1987; Wilkinson, 1984). The oil phase first becomes discontinuous at the same point where water becomes continuous across the medium. This is also true for rectangular channels where wetting phase cannot move simultaneously together with nonwetting phase through thick films connecting water surrounding adjacent pillars. The reason is that the condition for connecting the wetting phase between pillars is also the condition for snap off that blocks throat to nonwetting phase (Rossen, 2003). The relative-permeability curves cross at zero relative permeability rather than above as in rock (Rossen & Kumar, 1992). Thus, the k_{rw} factor in a micromodel is very different than that in rock. The value of N_{ca} in equation (2) must be much larger for micromodels than that in equation (1) under the same conditions, by a factor different from that for geological porous media. Thus, one is especially likely to misinterpret mobilization in micromodels, based on the value of N_{ca} defined in equation (1). For instance, capillary numbers around 10^{-5} as defined by equation (1) correspond to considerable mobilization in micromodels, for example, S_{nw} of about 10–15% (Buchgraber et al., 2012; Geistlinger et al., 2015). This greatly overestimates mobilization implied by similar capillary numbers in geological porous media.

Microfluidic devices are particularly useful in revealing the fundamentals of transport of fluids in porous media, in that flow processes and phase-interaction dynamics can be observed directly. To describe mobilization in micromodels, we propose in this study a new definition of capillary number, taking into account the pore geometry of 2-D microfluidic networks.

AlQuaimi and Rossen (2017) recently proposed a mobilization condition for the nonwetting phase in rough-walled fractures, from a force balance on a trapped ganglion. Here we derive a new N_{ca} definition for micromodels using a method similar to theirs. The geometrical factors controlling capillary trapping in micromodels differ fundamentally from those in fractures. In a fracture, aperture-depth variation along a flow path dominates the capillary pressure between nonwetting and wetting phases. In micromodels, where aperture depth is usually uniform, capillary pressure is controlled by the widths of pore throats and pores, perpendicular to the etching. The validity of the new definition is then tested using published data obtained in a variety of micromodels varying in the pore geometry. The introduction pore microstructure in the new definition overcomes the large scatter in the CDC that occurs with the conventional definitions.

2. New Capillary Number Definition

In this section, we present the derivation of the new N_{ca} definition for micromodels, starting with a force balance on a trapped nonwetting ganglion illustrated in Figure 1. We then illustrate how to estimate all the parameters needed in the new definition.

2.1. Derivation From a Force Balance

The residual nonaqueous phase at the end of a displacement consists of discrete blobs trapped behind pore throats. Our study focuses on the mobilization of the nonwetting phase as schematically illustrated in Figure 1.

The nonwetting ganglion trapped in Figure 1 is subject to the following forces: pressure, gravity, and capillary resistance. The mobilization of the ganglion in Figure 1 is thus a competition of pressure/gravitational force, sometimes called viscous force, and capillary resistance (Larson et al., 1977).

We define a dimensionless factor N_{ca}, as a ratio of viscous force, F_v, to capillary resistance, F_c:

$$N_{ca} = \frac{F_v}{F_c}. \tag{4}$$

At the onset of mobilization, the leading edge of the ganglion resides in the pore throat and the trailing edge in the pore body. Such a configuration yields different curvatures at the leading and trailing edges, leading to capillary resistance to the mobilization. The capillary pressure across any interface is described by the Laplace equation:

$$P_c = \sigma\left(\frac{1}{r_1} + \frac{1}{r_2}\right), \tag{5}$$

where σ is the interfacial tension and r_1 and r_2 the principle radii of curvature of the interface.

Lenormand et al. (1983) derived the capillary pressure across an interface in a rectangular channel:

$$P_c \cong 2\sigma\left(\frac{1}{x} + \frac{1}{y}\right), \tag{6}$$

where x and y represent the height and width of the rectangular cross section. The capillary-pressure difference, Δp_c, across the curved interfaces at the leading and trailing edges of the ganglion is then given by

$$F_c = \Delta p_c = \sigma\left(\frac{2\cos\theta}{W_t} - \frac{2\cos\theta}{W_b}\right), \tag{7}$$

where θ is the contact angle and W_t and W_b the pore-throat width and pore-body diameter (as viewed from above) as shown in Figure 1, respectively. The channel depth, d_z, is uniform and thus drops out in equation (7).

The viscous force, F_v, across a trapped ganglion of length L_g as in Figure 1 is given by

$$F_v \cong |\nabla\Phi| L_g, \tag{8}$$

where $|\nabla\Phi|$ is the magnitude of the macroscopic flow-potential gradient, the combined effects of pressure p, and gravity. For the remainder of this derivation, for simplicity, we assume the flow is horizontal, and $|\nabla\Phi| = |\nabla p|$.

We assume for simplicity that both the ganglion length L_g and its distribution scale with L_p, the length of a pore (roughly identical to pore-body diameter W_b in the networks considered). For the experiments analyzed here (Figure A1 in Appendix A), the characteristic ganglion length L_g at residual state at the end of a displacement is a factor of about 1.1–1.4 times W_b. Then we substitute L_p for L_g in the remainder of the derivation.

The viscous force F_v required to mobilize a ganglion of length L_p has to overcome the capillary resistance F_c:

$$F_v > F_c, \text{ or } |\nabla p| \cdot L_p > \sigma\left(\frac{2\cos\theta}{W_t} - \frac{2\cos\theta}{W_b}\right). \tag{9}$$

The left side of equation (9) divided by the right side yields a criterion for the mobilization in terms of the dimensionless capillary number N_{ca}:

$$N_{ca} \equiv \frac{F_v}{F_c} = \left(\frac{|\nabla p|}{\sigma\cos\theta}\right)\left[\frac{L_p W_t}{2\left(1 - \frac{W_t}{W_b}\right)}\right] > 1. \tag{10}$$

The second term in brackets describes the impact of the geometric characteristics of the pore network on the displacement of residual nonwetting phase. Since all the parameters involved in the bracketed term are

related to the geometry of the micromodel, the second term in equation (10) should be a constant for a given micromodel, independent of fluid properties. Note that our derivation is based on a ganglion one pore in length. Ganglia several pores long would be mobilized at N_{ca} somewhat smaller than unity. More fundamentally, the derivation assumes that the distribution of ganglion lengths for all micromodels scales with the length of a single pore. This assumption facilitates the calculation of the new N_{ca} in equation (10) based only on microfluidic geometry, without needing to perform flow experiments in advance.

2.2. Comparison of the New and Conventional N_{ca}

Nearly all publications concerning the CDC for micromodels apply the conventional N_{ca} definitions. To reveal the relation between the new definition for micromodels and the conventional definition for porous rock and for the convenience of reexamining published data from micromodels, we derive a conversion factor between the two definitions.

Mathematically, the conversion is done via introducing permeability k into the new definition in equation (10). Physically, this requires one to relate k to the pore geometry of a micromodel. Since the link between the permeability and pore microstructure is complex, we estimated k of a micromodel by comparison to a smooth slit. Specifically, the permeability, k_s, of a smooth slit of aperture d_z is given by (Tsang, 1992; van Golf-Racht, 1982; Zimmerman & Bodvarsson, 1996):

$$k_s = \frac{d_z^2}{12}, \tag{11}$$

where subscript s denotes the slit, and d_z represents the aperture of the slit.

Channel depth d_z is usually a fixed constant for a given micromodel. Permeability in a micromodel, k, is reduced first by the porosity, because only the pores can conduct flow. For a simple reference case of wide, shallow, straight, smooth channels, permeability would be $\left[\left(d_z^2/12\right)\cdot\varphi\right]$, where φ is the porosity. If etching depth is comparable to channel width or the channel network geometry is more complex, then k would be reduced by more than φ. This additional reduction due to geometrical issues we incorporate into a factor ς:

$$k = \left(\frac{d_z^2}{12}\right)\cdot(\varphi\varsigma), \tag{12}$$

where ς is a factor incorporating several effects, as is geometric tortuosity for 3-D porous media (Doyen, 1988; Ghanbarian et al., 2013). We use this factor here only to allow us to relate the new definition of N_{ca} to the conventional definition based on permeability, to illustrate their difference.

Introducing the relation defined by equation (12) into the second bracketed term in equation (10) yields

$$\begin{aligned}\frac{L_p W_t}{2\left(1-\frac{W_t}{W_b}\right)} &= \left(\frac{d_z^2}{12}\varphi\varsigma\right)\left(\frac{1}{\frac{d_z^2}{12}\varphi\varsigma}\right)\frac{L_p W_t}{2\left(1-\frac{W_t}{W_b}\right)} \\ &= k\cdot\left[\left(\frac{12}{2}\right)\left(\frac{W_t}{d_z}\right)^2\left(\frac{L_p}{W_t}\right)\frac{1}{\left(1-\frac{W_t}{W_b}\right)(\varphi\varsigma)}\right].\end{aligned} \tag{13}$$

Replacing the bracketed term in equation (10) with the right side of equation (13) and grouping all the geometrical factors together produce an expression for the new N_{ca} equivalent to that in equation (10):

$$N_{ca} = \left(\frac{k|\nabla p|}{\sigma\cos\theta}\right)\left[\left(\frac{12}{2}\right)\left(\frac{W_t}{d_z}\right)^2\left(\frac{L_p}{W_t}\right)\frac{1}{\left(1-\frac{W_t}{W_b}\right)(\varphi\varsigma)}\right], \tag{14}$$

where the first term in parentheses is the conventional definition in equation (2). The second part, in brackets, describes the impact of pore microstructure.

Table 1
Summary of Parameters Needed for Calculation of the New N_{ca}

	Model parameters	Remarks
Geometrical factors	Characteristic pore-throat width, W_t	Statistical average of pore-throat distribution
	Characteristic pore-body diameter, W_b	Statistical average of pore-body distribution
	Pore length, L_p	Roughly identical to W_b in the networks considered here
Fluid and media properties	Wettability, indicated by contact angle, θ	Measured in lab
	Interfacial tension between phases,σ	Measured in lab
Flow data	Pressure gradient, ∇p	Measured via flow experiments

We define the second bracketed term in equation (14) as the geometric term G:

$$G \equiv \left(\frac{12}{2}\right)\left(\frac{W_t}{d_z}\right)^2\left(\frac{L_p}{W_t}\right)\frac{1}{\left(1-\frac{W_t}{W_b}\right)(\varphi\varsigma)}. \tag{15}$$

The factors in G can be estimated from image analysis of a micromodel, the depth of the etching and a value for permeability. The value of G is fixed for a specific micromodel. After knowing G, one can convert the new and conventional definitions.

2.3. Calculation of Parameters in the New N_{ca}

The parameters needed for the calculation of the new N_{ca} (equation (10)) include pressure gradient ∇p, interfacial tension σ, contact angle θ, characteristic pore-throat width W_t, characteristic pore-body diameter W_b, and pore length L_p (Table 1 below). The geometrical factors, W_t, W_b, and L_p, can be obtained via image analysis of a micromodel. One can calculate the new N_{ca} in equation (10) after acquiring the parameters summarized in Table 1.

3. Test of the New N_{ca} Definition

This section illustrates first the major issues concerning the direct application of the conventional N_{ca} definitions to analyze mobilization in micromodels (Figure 2). The validity of the new N_{ca} definition is then verified using the same data (Figure 3).

Data from published experiments that represent a variety of micromodels differing in their pore geometry are used to test this model. Table 2 summarizes all the key parameters depicting the network geometry and properties of micromodels used in these studies. These include, in particular, the geometric factors characterizing the microstructure of pore throats and pore bodies and pore length. The values of the geometric parameters in Table 2 are either given in the publications or estimated from image analysis of the micromodel (Ibrahim, 2009; Jeong & Corapcioglu, 2003; Yeganeh et al., 2016). The values of ς are calculated via equation (12) based on k provided in the respective studies in Table 2, which then gives the values of G defined in equation (15). Based on the conversion in equation (14), one can then translate the conventional N_{ca} to the new N_{ca}, to check the effectiveness of the new definition. The studies of Jones et al. (2018) and of Kawale et al. (2017) do not provide two-phase flow data but allow geometric analysis of the micromodels. We present the values of G for these cases, to illustrate the expected impact of pore geometry if the CDC were measured with these micromodels.

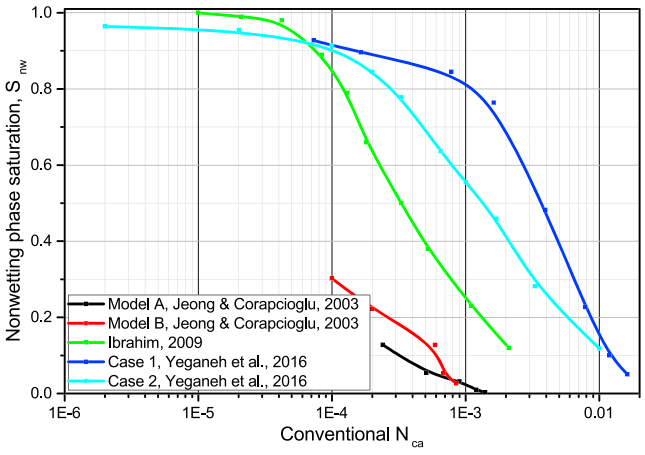

Figure 2. Capillary-desaturation curves using the conventional capillary number N_{ca} definitions. All the data shown here are adapted from data in publications. Note that the capillary-desaturation curve for micromodels results using the conventional definitions shows a large scatter, suggesting system-dependent.

Relatively few experimental studies provide the experimental details needed to estimate N_{ca} using equation (10), that is, permeability, pore geometry, wettability, and pressure gradient.

The CDCs shown in Figure 2 were collected from a variety of microfluidic studies (Ibrahim, 2009; Jeong & Corapcioglu, 2003, 2005; Yeganeh et al., 2016). Different conventional N_{ca} definitions were

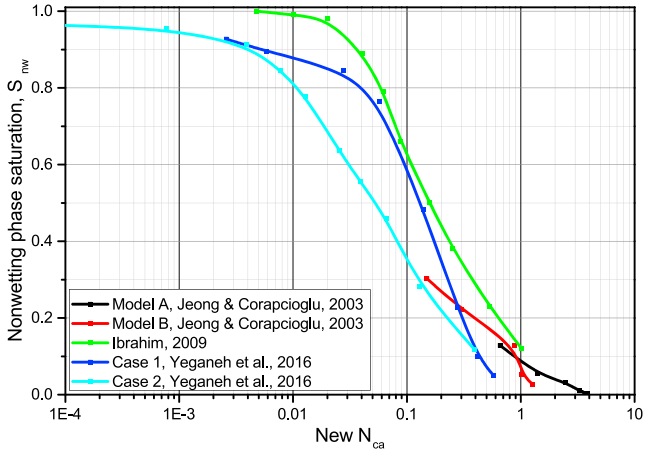

Figure 3. Capillary-desaturation curves using the new capillary number N_{ca} definition in equation (10), using data in Figure 2.

applied in these studies. For instance, Jeong and Corapcioglu (2003) used a definition similar to equation (1), but including contact angle and ignoring porosity, given by

$$N_{ca} = \frac{q\mu_a}{\sigma\cos\theta} = \frac{kk_{rw}|\nabla p|}{\sigma\cos\theta}, \tag{16}$$

where q and μ_a represent in their study the superficial velocity and viscosity of the displacing fluid and k and k_{rw} the absolute and relative permeability, respectively.

The studies of Ibrahim (2009) and Yeganeh et al. (2016) employed the following definition:

$$N_{ca} = \frac{v\mu}{\sigma\cos\theta}. \tag{17}$$

This definition is a factor $(1/\varphi)$ times of that in equation (16). We converted all the data, for the convenience of comparison, to the definition in equation (16) in Figure 2.

The parameters, θ, σ, and ∇p, are either taken or estimated from the publications. The key to the calculation of the new N_{ca} is the determination of the second bracketed term in equation (10). We estimated all the parameters in this term from image analysis of the micromodel based on pictures in the original publications. The characteristic pore-throat width, W_t, and pore-body length, L_p, are estimated by taking the average of their respective distributions. The channel depth, d_z, is given in the publications.

Figure 2 shows the CDCs based on data from five microfluidic devices in three studies, using the conventional definition of N_{ca} in equation (16). The data diverge by almost two orders of magnitude. The large scatter in Figure 2 suggests that the CDC using the N_{ca} in terms of $v\mu$ or $u\mu$ is system-dependent. Thus, neither of the two definitions in equations (16) and (17) works for micromodels.

The same data in Figure 2 were then replotted in Figure 3 using the new definition in equation (10). Calculating the new N_{ca} requires ∇p, which was not reported in the studies of Figure 2. These are the only studies where we can find the data we need. Equation (14), by incorporating Darcy's velocity, is equivalently rearranged to

$$N_{ca} = \left(\frac{u\mu}{\sigma\cos\theta}\right)\frac{1}{k_{rw}}\left[\left(\frac{12}{2}\right)\left(\frac{W_t}{d_z}\right)^2\left(\frac{L_p}{W_t}\right)\frac{1}{\left(1-\frac{W_t}{W_b}\right)(\varphi\varsigma)}\right]. \tag{18}$$

Through equation (18), one can translate the values of conventional N_{ca} from equation (16) in Figure 2 to the new N_{ca}. The quantities in the large brackets can be determined from image analysis of the micromodels,

Table 2
An Overview of Micromodel Parameters Collected From Microfluidic Studies in the Publications

Published studies		Micromodel geometrical factors				Micromodel properties		Adjustable factor ς	G values
		W_t (μm)	W_b (μm)	L_p (μm)	d_z (μm)	k (μm^2)	φ		
Kawale et al. (2017)	Aligned squares	217	307	307	120	204	0.69	0.246	558
	Staggered squares	109	415	415	120	180	0.71	0.211	169
	Aligned circles	162	338	338	120	214	0.71	0.251	246
	Staggered circles	162	338	338	12	179	0.71	0.210	293
Jones et al. (2018)		13	60	60	5	0.72	0.71	0.488	691
Jeong and Corapcioglu (2003)	Model A	152	326	326	130	17	0.27	0.045	2741
Jeong and Corapcioglu (2003)	Model B	130	272	272	130	22.5	0.28	0.057	1505
Ibrahim (2009)		64	210	210	150	20	0.50	0.022	483
Yeganeh et al. (2016)	Case 1	86	156	156	110	362	0.59	0.614	41
Yeganeh et al. (2016)	Case 2	86	155	155	110	362	0.59	0.614	41

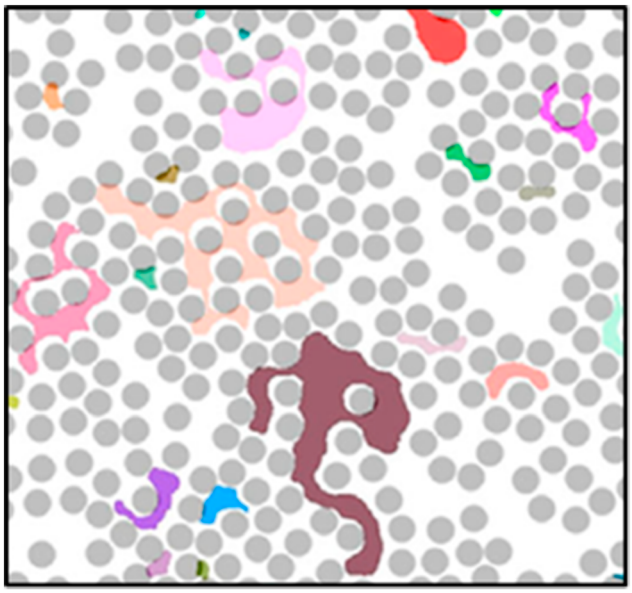

Figure 4. Distribution of trapped ganglia in a highly heterogeneous network, adapted from Geistlinger et al. (2015). Gray circles represent pillars on the way, shaping flow channels, and colored clusters represent trapped gas ganglia.

except for ς which is calculated here from measured k through equation (12). We do not know the value of k_{rw} in these studies, or how it varies with S_{nw}. In Figure 3, we assume a value of 1 so as to examine the shape of the new model using the published data in Figure 2. The simplification implies that the values of N_{ca} in Figure 3 should be somewhat larger than shown.

Figure 3 shows that the new N_{ca} definition gives a much better match to the data in micromodels, in spite of the unknown factor k_{rw} and the simplifying assumption concerning the ganglion-length distribution. The improved fit of the new N_{ca} to data confirms its validity by yielding a consistent trend in the CDC. As the k_{rw} factor was ignored in the translation of conventional in Figure 2 to new N_{ca} in Figure 3, the true CDC may move to the right somewhat from Figure 3, though allowing for ganglia longer than a pore would tend to move it back to the left. The consistent trend in the CDC demonstrates the validity of the new N_{ca} for evaluating mobilization or trapping of the nonwetting phase in microfluidic studies. In addition, the values of new N_{ca} in Figure 3 are tens to thousands of times greater than those in Figure 2, as implied by the values of G in Table 2. These confirm the overestimation of the conventional CDC using the definitions in equations (1) and (2) for mobilization in micromodels.

The complications concerning ς are glossed over in the conventional N_{ca} definitions in equations (1) and (2) as well. Nonetheless, they work remarkably well, yielding a consistent trend in the CDC for geological porous media. Here we discuss k, k_{rw}, and ς in relating the two definitions using equations (14) or (18) only to illustrate the difference between the new and conventional definitions. The new N_{ca} model we suggest in equation (10) does not include k, k_{rw}, or ς.

4. Discussion and Future Work

It is the dependence of the new N_{ca} on pore geometry as described in the bracketed term in equation (18) that shifts the separate CDC's in Figure 2 to converge to Figure 3. The large values of G (Table 2) explain the reason why the value of N_{ca} needed to mobilize the nonwetting phase in micromodels using the conventional definition is much less than that in rock (Buchgraber et al., 2012; Geistlinger et al., 2015). The conventional definition is misleading, when using micromodel results to interpret displacements in porous rock.

All the data we examined were obtained in fairly homogeneous or slightly heterogeneous networks (Figure A1 in Appendix A). The assumption of ganglion length scaling with one pore in length is consistent with experimental observations for these micromodels. For very heterogeneous networks, the distribution of ganglion length is complex, as illustrated in Figure 4, adapted from Geistlinger et al. (2015). To apply the new definition in such a context, one may need to capture the distribution of L_g to describe the mobilization effectively, since the distribution of ganglia affects the capillary resistance significantly. Some studies (Iglauer et al., 2010; Iglauer, Wülling, et al., 2011, Iglauer, Paluszny, et al., 2011) show that the distribution of L_g for a range of N_{ca} values near the onset of mobilization follows a universal power law predicted from percolation theory.

Figure 3 shows that mobilization starts for values of the new N_{ca} less than one. The derivation is based on a trapped ganglion a single pore long. In a displacement process, the distribution of ganglion lengths includes many ganglia several pores in length. The viscous force required to mobilize those ganglia is much less than that for a ganglion filling a single pore; they are mobilized at $N_{ca} < 1$. The new definition of N_{ca} in equation (10) in principle reflects the maximum effort required to mobilize an isolated trapped ganglion. Also accounting for the factor k_{rw} in equation (18) would increase the values of new N_{ca}.

The CDC gives the correlation between S_{nw} and N_{ca}, which is an analysis done after the experiment. To predict the mobilization or trapping in terms of a dimensionless N_{ca}, a physical model is then needed to describe the relation of S_{nw} as a function of N_{ca}. This can enhance our understanding about the fundamentals of CDC. Furthermore, it is useful for optimizing an operation designed to maximize the mobilization efficiency in oil recovery, removal efficiency of NAPL in contaminated ground water and soils, or the trapping efficiency of CO_2 in CCUS.

5. Conclusions

Mobilization of residual nonwetting phase in 2-D micromodels is very different from that in 3-D geological porous media. Consequently, the conventional N_{ca} definitions proposed for 3-D pore networks do not apply to micromodel results. Direct application may lead to incorrect conclusions for fluid transport in geological formations.

A new capillary number (N_{ca}) definition, derived from the force balance on a nonwetting ganglion trapped by capillarity, is proposed for micromodels.

The new definition incorporates the impact of pore geometry on mobilization. The geometrical factors introduced can be estimated from image analysis of the network of a micromodel, without performing flow experiments. The improved fit of the new N_{ca} to published data supports its validity by yielding a consistent trend in CDC, suggesting the crucial role that pore geometry plays in mobilization.

The new N_{ca} definition works better than the conventional definitions for the evaluation of mobilization or trapping efficiency of nonwetting phase in microfluidics in a variety of processes: removal of NAPL contaminants in soils and aquifers, displacement of oil in petroleum industry, and trapping of CO_2 in CCUS.

A conversion factor between the new and conventional N_{ca} definitions is provided, to compare the difference and facilitate reexamining published data in micromodels.

Further experimental studies are needed to demonstrate the validity of a CDC based on equation (10) for a wider range of microfluidic network geometries.

Nomenclature

d_z = channel depth of a micromodel, m
F_c = capillary force, Pa
F_v = viscous force, Pa
G = geometric factor for micromodels, dimensionless
k = absolute permeability, m^2
k_s = permeability of a smooth slit of aperture d_z, m^2
k_{rw} = relative permeability of wetting phase, dimensionless
L_g = length of a trapped ganglion, m
L_p = length of one pore, m
N_{ca} = capillary number, dimensionless
P_c = capillary pressure, Pa
$|\nabla p|$ = magnitude of macroscopic pressure gradient, Pa/m
Δp_c = capillary-pressure difference over curved interface of a ganglion, Pa
q = superficial velocity, m/s
r_1, r_2 = principle radii of curvature, m
μ,μ_a = viscosity of displacing fluid, Pa.s
u, v = superficial and interstitial velocity of displacing fluid, m/s
x, y = width and height of cross-section of a rectangular channel, m
W_b = characteristic pore-body diameter, m
W_t = characteristic pore-throat width, m
σ = interfacial tension over an interface, N/m
φ = porosity, a fraction
$|\nabla\Phi|$ = magnitude of macroscopic flow-potential gradient, Pa/m

θ = contact angle, dimensionless as measured in radians
ς = adjustable factor to relate permeability and pore geometry, dimensionless

Subscripts and superscripts

b = pore body
c = capillarity
g = ganglion
t = pore throat
v = viscous force
z = channel depth

Appendix A: Microfluidic Devices in the Literature

Figure A1 shows images of the microfluidic devices from the literature that were used to obtain the data in Figures 2 and 3.

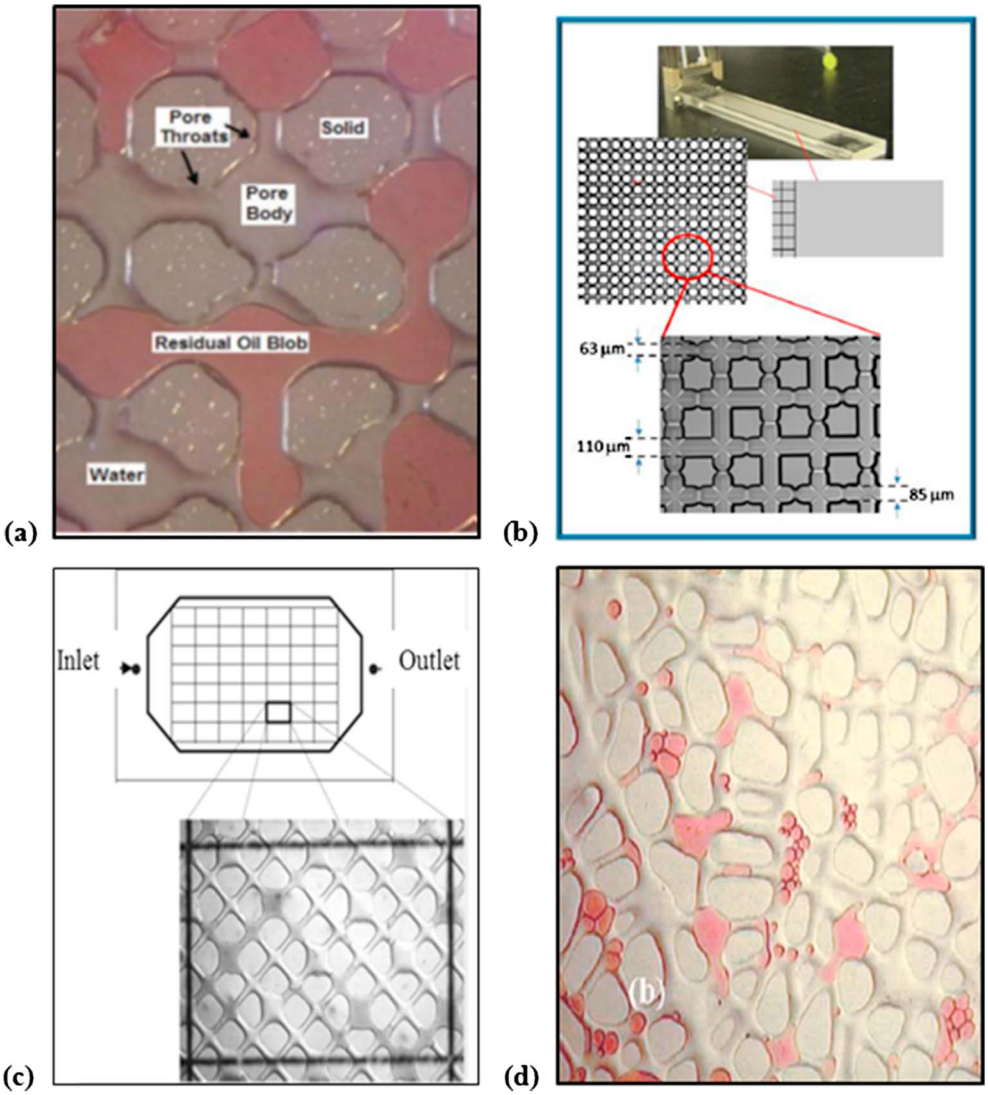

Figure A1. Pore geometry of the microfluidic devices as used in Figures 2 and 3: (a) Ibrahim (2009); (b) Yeganeh et al. (2016); (c and d) model A and B, respectively, in Jeong and Corapcioglu (2003).

Acknowledgments

This work was supported by the Joint Industry Project on Foam for Enhanced Oil Recovery at Delft University of Technology and by a scholarship from the China Scholarship Council. Sebastien Vincent-Bonnieu would like to thank Shell Global Solutions International B.V. for their review on this article and their permission for publication.

References

Abrams, A. (1975). *The influence of fluid viscosity, interfacial tension, and flow velocity on residual oil saturation left by waterflood* (Vol. 15, pp. 437–447). Richardson, TX: Society of Petroleum Engineers. https://doi.org/10.2118/5050-PA

AlQuaimi, B., & Rossen, W. (2017). New capillary number definition for displacement of residual nonwetting phase in natural fractures. *Geophysical Research Letters*, *44*, 5368–5373. https://doi.org/10.1002/2017GL073211

Al-Shalabi, E., Sepehrnoori, K., Pope, G., & Mohanty, K. (2014). A fundamental model for predicting oil recovery due to low salinity water injection in carbonate rocks. Presented at the SPE Energy Resources Conference, Society of Petroleum Engineers.

Bethel, F. T., & Calhoun, J. C. (1953). *Capillary desaturation in unconsolidated beads, Journal of Petroleum Technology* (Vol. 5, pp. 197–202). Houston, TX: Society of Petroleum Engineers. https://doi.org/10.2118/953197-G

Brownell, L. E., & Katz, D. L. (1947). Flow of fluids through porous media. 2. Simultaneous flow of 2 homogeneous phases. *Chemical Engineering Progress*, *43*(11), 601–612.

Buchgraber, M., Kovscek, A. R., & Castanier, L. M. (2012). A study of microscale gas trapping using etched silicon micromodels. *Transport in Porous Media*, *95*(3), 647–668. https://doi.org/10.1007/s11242-012-0067-0

Chatzis, I., & Dullien, F. A. L. (1977). *Modelling pore structure by 2-D and 3-D networks with application to sandstones*. Petroleum Society of Canada. PETSOC-77-01-09. Calgary, Alberta, Canada. https://doi.org/10.2118/77-01-09

Chatzis, I., Morrow, N. R., & Lim, H. T. (1983). *Magnitude and detailed structure of residual oil saturation, Society of Petroleum Engineers Journal* (Vol. 230, pp. 311–326). Richardson, TX: Society of Petroleum Engineers. https://doi.org/10.2118/10681-PA

Dombrowski, H., & Brownell, L. (1954). Residual equilibrium saturation of porous media. *Industrial and Engineering Chemistry*, *46*(6), 1207–1219. https://doi.org/10.1021/ie50534a037

Doyen, P. M. (1988). Permeability, conductivity, and pore geometry of sandstone. *Journal of Geophysical Research*, *93*(B7), 7729–7740. https://doi.org/10.1029/JB093iB07p07729

Foster, W. R. (1973). *A low-tension waterflooding process, Journal of Petroleum Technology* (Vol. 25, pp. 205–210). Houston, TX: Society of Petroleum Engineers. https://doi.org/10.2118/3803-PA

Franklin, M. (1994). *Scale-up of miscible flood processes for heterogeneous reservoirs*. Standford, CA: Petroleum Engineering Department, Standford University.

Geistlinger, H., Ataei-Dadavi, I., Mohammadian, S., & Vogel, H.-J. (2015). The impact of pore structure and surface roughness on capillary trapping for 2-D and 3-D porous media: Comparison with percolation theory. *Water Resources Research*, *51*, 9094–9111. https://doi.org/10.1002/2015WR017852

Geistlinger, H., Lazik, D., Krauss, G., & Vogel, H.-J. (2009). Pore-scale and continuum modeling of gas flow pattern obtained by high-resolution optical bench-scale experiments. *Water Resources Research*, *45*, W04423. https://doi.org/10.1029/2007WR006548

Ghanbarian, B., Hunt, A. G., Ewing, R. P., & Sahimi, M. (2013). Tortuosity in porous media: A critical review. *Soil Science Society of America Journal*, *77*(5), 1461–1477. https://doi.org/10.2136/sssaj2012.0435

Green, D. W., & Willhite, G. P. (1998). In H. L. Doherty (Ed.), *Memorial Fund of AIMEEnhanced oil recovery* (Vol. 6). Richardson, TX: Society of Petroleum Engineers.

Ibrahim, A. S. (2009). *Investigation of the mobilization of residual oil using micromodels*. Presented at the SPE Annual Technical Conference and Exhibition, Society of Petroleum Engineers, SPE-129515-STU.

Iglauer, S., Favretto, S., Spinelli, G., Schena, G., & Blunt, M. J. (2010). X-ray tomography measurements of power-law cluster size distributions for the nonwetting phase in sandstones. *Physical Review E*, *82*(5), 56315. https://doi.org/10.1103/PhysRevE.82.056315

Iglauer, S., Wülling, W., Pentland, C. H., Al-Mansoori, S. K., & Blunt, M. J. (2011). *Capillary-trapping capacity of sandstones and sandpacks, Society of Petroleum Engineering Journal* (Vol. 16, pp. 778–78). Richardson, TX: Society of Petroleum Engineers. https://doi.org/10.2118/120960-PA

Iglauer, S., Paluszny, A., Pentland, C. H., & Blunt, M. J. (2011). Residual CO_2 imaged with X-ray micro-tomography. *Geophysical Research Letters*, *38*, L21403. https://doi.org/10.1029/2011GL049680

Jeong, S.-W., & Corapcioglu, M. Y. (2003). A micromodel analysis of factors influencing NAPL removal by surfactant foam flooding. *Journal of Contaminant Hydrology*, *60*(1–2), 77–96. https://doi.org/10.1016/S0169-7722(02)00054-2

Jeong, S.-W., & Corapcioglu, M. Y. (2005). Force analysis and visualization of NAPL removal during surfactant-related floods in a porous medium. *Journal of Hazardous Materials*, *126*(1-3), 8–13. https://doi.org/10.1016/j.jhazmat.2005.06.015

Johnson, P. C., Johnson, R. L., Bruce, C. L., & Leeson, A. (2001). Advances in in situ air sparging/biosparging. *Bioremediation Journal*, *5*(4), 251–266. https://doi.org/10.1080/20018891079311

Jones, S., Getrouw, N., & Vincent-Bonnieu, S. (2018). Foam flow in a model porous medium: I. The effect of foam coarsening. *Soft Matter*, *14*(18), 3490–3496.

Juanes, R., Spiteri, E. J., Orr, F. M., & Blunt, M. J. (2006). Impact of relative permeability hysteresis on geological CO_2 storage. *Water Resources Research*, *42*, W12418. https://doi.org/10.1029/2005WR004806

Kao, C. M., Chen, C. Y., Chen, S. C., Chien, H. Y., & Chen, Y. L. (2008). Application of in situ biosparging to remediate a petroleum-hydrocarbon spill site: Field and microbial evaluation. *Chemosphere*, *70*(8), 1492–1499. https://doi.org/10.1016/j.chemosphere.2007.08.029

Kawale, D., Marques, E., Zitha, P. L., Kreutzer, M. T., Rossen, W. R., & Boukany, P. E. (2017). Elastic instabilities during the flow of hydrolyzed polyacrylamide solution in porous media: Effect of pore-shape and salt. *Soft Matter*, *13*(4), 765–775. https://doi.org/10.1039/C6SM02199A

Lake, L. W., Johns, R. T., Rossen, W. R., & Pope, G. (2014). *Fundamentals of enhanced oil recovery*. Richardson, TX: Society of Petroleum Engineers.

Larson, R., Scriven, L., & Davis, H. (1977). Percolation theory of residual phases in porous media. *Nature*, *268*(5619), 409–413. https://doi.org/10.1038/268409a0

Lenormand, R., Zarcone, C., & Sarr, A. (1983). Mechanisms of the displacement of one fluid by another in a network of capillary ducts. *Journal of Fluid Mechanics*, *135*(1), 337–353. https://doi.org/10.1017/S0022112083003110.

Mohanty, K. K., Davis, H. T., & Scriven, L. E. (1987). Physics of oil entrapment in water-wet rock. SPE-9406-PA. https://doi.org/10.2118/9406-PA

Moore, T. F., & Slobod, R. L. (1955). *Displacement of oil by water-effect of wettability, rate, and viscosity on recovery*. SPE-502-G. Richardson, TX: Society of Petroleum Engineers. https://doi.org/10.2118/502-G

Pennell, K. D., Pope, G. A., & Abriola, L. M. (1996). Influence of viscous and buoyancy forces on the mobilization of residual tetrachloroethylene during surfactant Flushing. *Environmental Science & Technology*, *30*(4), 1328–1335. https://doi.org/10.1021/es9505311

Pope, G., Wu, W., Narayanaswamy, G., Delshad, M., Sharma, M., & Wang, P. (2000). Modeling relative permeability effects in gas-condensate reservoirs with a new trapping model. *SPE Reservoir Evaluation & Engineering*, *3*(02), 171–178. https://doi.org/10.2118/62497-PA

Reed, R. L., & Healy, R. N. (1977). Some physicochemical aspects of microemulsion flooding: A review. In *Improved oil recovery by surfactant and polymer flooding* (pp. 383–437). Amsterdam, Netherlands: Elsevier. https://doi.org/10.1016/B978-0-12-641750-0.50017-7

Rodríguez de Castro, A., Shokri, N., Karadimitriou, N., Oostrom, M., & Joekar-Niasar, V. (2015). Experimental study on nonmonotonicity of capillary desaturation curves in a 2D pore network. *Water Resources Research*, *51*, 8517–8528. https://doi.org/10.1002/2015WR017727

Ross, C. M., & Kovscek, A. R. (2002). *Pore microstructure and fluid distribution in a diatomaceous reservoir*. In *SPE-75190-MS*. Richardson, TX: Society of Petroleum Engineers. https://doi.org/10.2118/75190-MS

Rossen, W. R. (2003). A critical review of roof snap-off as a mechanism of steady-state foam generation in homogeneous porous media. *Colloids and Surfaces A: Physicochemical and Engineering Aspects*, *225*(1–3), 1–24. https://doi.org/10.1016/S0927-7757(03)00309-1

Rossen, W. R., & Kumar, A. T. A. (1992). *Single- and two-phase flow in natural fractures*. In *SPE-24915-MS*. Richardson, TX: Society of Petroleum Engineers. https://doi.org/10.2118/24915-MS

Sheng, J. (2010). *Modern chemical enhanced oil recovery: Theory and practice*. Houston, TX: Gulf Professional Publishing.

Tsang, Y. (1992). Usage of "equivalent apertures" for rock fractures as derived from hydraulic and tracer tests. *Water Resources Research*, *28*(5), 1451–1455. https://doi.org/10.1029/92WR00361

van Golf-Racht, T. D. (1982). *Fundamentals of fractured reservoir engineering* (Vol. 12). Amsterdam, Netherlands: Elsevier.

Wilkinson, D. (1984). Percolation model of immiscible displacement in the presence of buoyancy forces. *Physical Review A*, *30*(1), 520–531. https://doi.org/10.1103/PhysRevA.30.520

Yeganeh, M., Hegner, J., Lewandowski, E., Mohan, A., Lake, L. W., Cherney, D., Arben Jusufi et al. (2016). Capillary desaturation curve fundamentals. Presented at the SPE Improved Oil Recovery Conference, SPE-179574-MS. https://doi.org/10.2118/179574-MS

Zimmerman, R. W., & Bodvarsson, G. S. (1996). Hydraulic conductivity of rock fractures. *Transport in Porous Media*, *23*(1), 1–30.